# RSC Advances

This is an *Accepted Manuscript*, which has been through the Royal Society of Chemistry peer review process and has been accepted for publication.

*Accepted Manuscripts* are published online shortly after acceptance, before technical editing, formatting and proof reading. Using this free service, authors can make their results available to the community, in citable form, before we publish the edited article. This *Accepted Manuscript* will be replaced by the edited, formatted and paginated article as soon as this is available.

You can find more information about *Accepted Manuscripts* in the **Information for Authors**.

ROYAL SOCIETY
OF **CHEMISTRY**

www.rsc.org/advances

1    Solar photocatalytic ozonation of emerging contaminants detected in municipal

2    wastewater treatment plant effluents by magnetic MWCNTs/TiO$_2$ nanocomposites

3                    Lian Yu[1],*, Dongsheng Wang[2], Daiqi Ye[1]

4    [1]College of Environment and Energy, South China University of Technology,

5    Guangzhou 510006, China

6    [2]State key Laboratory of Environmental Aquatic Chemistry, Research Center for

7    Eco-Environmental Sciences, Chinese Academy of Sciences, P.O. Box 2871, Beijing

8    100085, China

9    **Abstract**

10    Magnetically separable catalyst with high solar photocatalytic ozonation activity

11    was successfully synthesized. First maghemite and then titania (anatase) nanoparticles

12    were deposited onto the multiwalled carbon nanotubes (MWCNTs) by

13    co-precipitation and sol-gel methods. The synthesized catalysts were characterized by

14    XRD, N$_2$ adsorption/desorption, TEM, XPS and VSM, and were applied for the

15    removal of emerging contaminants (ECs) existing in urban wastewater through

16    photocatalytic ozonation. Ozone alone can completely remove the mixture of the four

17    ECs in the water, but the mineralization degree was very low (44.9%). Photocatalytic

18    oxidation led to a higher level of mineralization (48.3% TOC removal) in the

19    experimental conditions, but some intermediate products such as phenolic compounds

20    and carboxylates which are toxic and difficult to degrade generated during

21    photocatalytic oxidation process. Photocatalytic ozonation led to the highest removal

22    efficiency for TOC (65.7%), which suggested lower concentration of intermediate

*Corresponding author. Tel.: +8602039380519; Fax:
+8602039380519. E-mail addresses: yulian1987@126.com

23    products accumulated during photocatalytic ozonation, the integration of ozonation

24    and solar photocatalytic oxidation improved the mineralization efficiency.

25    **Keywords:** Ozonation; Photocatalytic oxidation; Photocatalytic ozonation; magnetic

26    MWCNTs/$TiO_2$; Emerging contaminants

27

## 1. Introduction

Emerging contaminants (ECs) are a group of synthetic compounds that have been recently detected in environmental waters. Although some inorganics, such as nanomaterials, can be considered as ECs, in most cases, ECs are organics, such as pharmaceuticals, perfluorinated compounds, hormones, endocrine disruptors, drinking water disinfection byproducts, sunscreens, algal toxins, pesticides and their degradation byproducts.[1-3] In recent years, the concentration of ECs that detected in environmental waters was tens of μg/L.[4-6] ECs can lead to a lot of risks, such as sterility, feminization of aquatic organisms and bacterial resistance, so ECs must be removed from environmental waters.

Recently, a lot of technologies are designed to remove ECs from water. They include advanced oxidation processes (AOPs) (combining strong oxidants, e.g. $H_2O_2$, with high energy sources, e.g. ultrasound (US) or ultraviolet (UV), and catalysts, e.g. photocatalysts (e.g. $TiO_2$) or $Fe^{2+}$, to produce hydroxyl radicals), membrane based technologies (nanofiltration, microfiltration, ultrafiltration and reverse osmosis), adsorption (e.g. active carbon) and ion exchange processes (e.g. resins).[7] Special attention has been paid to AOPs, in which the generated hydroxyl radicals ($^{\cdot}OH$) can oxidate almost any organic molecules.[7] Among AOPs, heterogeneous photocatalysis (UV/$TiO_2$) has attracted extensive attention for wastewater treatment.[8] The main drawback of heterogeneous photocatalysis is the highly operating costs resulting from electricity for the UV lamps used in photocatalysis. Therefore, more and more researches focused on photocatalysis that can be driven by sunlight.[9] Despite the

50    great potential of solar photocatalytic oxidation, some drawbacks (such as long

51    hydraulic detention time) have limited its practical use. A novel process, which

52    combines solar photocatalysis and ozone, can overcome these drawbacks, as it can

53    significantly increase the degradation rate of ECs.[10] The reason for this is likely due

54    to the adsorption of ozone onto the $TiO_2$ surface where it can trap electrons generated

55    from the conduction band of $TiO_2$, thus avoiding ineffective electron-hole

56    recombination, and at the same time generating ozonide radicals ($^{\cdot}O_3^{-}$), which can be

57    further transformed into hydroxyl radicals.[11-13]

58    Carbon nanotubes (CNTs), due to their specific physical, chemical and electronic

59    properties, have been used for advanced applications, such as catalysts or

60    reinforcements in composite materials,[14-17] CNTs are also excellent supports for

61    photocatalysts.[18,19] Taking advantage of the unique properties of MWCNTs, it has

62    been indicated that MWCNTs can promote the charge separation by trapping the

63    electrons that transferred from $TiO_2$, thus hindering charge recombination.[20] The

64    application of carbon materials for $TiO_2$ photodegradation of pollutants has been

65    reported, the enhanced performance of carbon/$TiO_2$ composites can be attributed to

66    several factors, such as the improvement of visible light absorption, the interfacial

67    electronic effects, the porosity of the carbon supports and the intrinsic photocatalytic

68    activity of certain carbons.[19,21-24] Another drawback of heterogeneous photocatalysis

69    is that it is difficult to remove the photocatalysts from water after the treatment.

70    Compared with centrifugation and filtration, magnetic separation is considered as a

71    rapid and effective method to separate nanomaterials from aqueous solution. The

72　decoration of MWCNTs with magnetic nanoparticles (such as magnetite and

73　maghemite) may be a promising method to separate MWCNTs from aqueous solution.

74　　　In this study, we report the preparation of a magnetic photocatalyst

75　(MWCNTs/TiO$_2$) which incorporates anatase TiO$_2$ nanoparticles onto magnetic

76　MWCNTs. The nanocomposites were characterized and used to degrade four

77　pharmaceutical compounds (selected as model ECs), i.e., atenolol (ATL),

78　hydrochlorothiazide (HCT), ofloxacin (OFX) and trimethoprim (TMP), which are

79　frequently detected in WWTPs' effluents and surface waters. Simulated solar-light

80　was used as radiation source and the removal efficiency of photocatalytic ozonation

81　was investigated and compared with those obtained from other AOPs, such as

82　photolysis (solar radiation), conventional ozonation (O$_3$) and solar photocatalytic

83　oxidation (catalyst/solar radiation). After the treatment, the magnetic MWCNTs/TiO$_2$

84　could be separated from the aqueous solution by an external magnetic field due to the

85　superparamagnetic behavior.

86　**2. Experimental**

87　2.1 Photocatalyst synthesis

88　　　The MWCNTs used in this study were purchased from Chengdu Institute of

89　Organic Chemicals, Chinese Academy of Science. MWCNTs were of the following

90　specifications: purity, ＞95%; outer diameter, 30-50 nm; inside diameter, 5-10 nm;

91　length, 10-20 μm. The purification process was performed to remove impurities and

92　modify the surface of MWCNTs with carbonyl and hydroxyl groups. The purification

93　process was accomplished by refluxing with concentrated nitric acid at 70□ for 12 h

94   under stirring conditions. The product was filtered and washed with distilled water,

95   and then dried overnight at 60□ under vacuum conditions.

96        Magnetic MWCNTs/TiO$_2$ (MCT) photocatalyst was prepared following the

97   method described previously, which comprises mainly two steps.[25] The first step was

98   the synthesis of magnetic γ-Fe$_2$O$_3$/MWCNTs using the co-precipitation and

99   subsequent oxidation method reported by Gupta et al..[26] A mixed solution of ferric

100  chloride hexahydrate (0.10 M) and ferrous chloride tetrahydrate (0.05 M) was

101  prepared. Subsequently, a specific amount of purified MWCNTs was added in the

102  mixed solution and stirred for 2 h. Then, at the temperature of 70□, NH$_4$OH (5.00 M)

103  solution was added drop wise to precipitate iron oxides. The pH of the mixture was

104  adjusted to 10.0 and then aged for 1 h under stirring. The product was separated by a

105  magnet, and then washed with distilled water and ethanol for several times,

106  respectively. The obtained composite was dried overnight at 60□ under vacuum

107  conditions and then calcined in a muffle furnace at 250□ for 2 h. The second stage

108  was the synthesis of magnetic MWCNTs/TiO$_2$ nanocomposites through a sol-gel

109  method.[27] A specific amount of γ-Fe$_2$O$_3$/MWCNTs was added into a mixture of

110  Ti(OBu)$_4$ (10.0 ml), anhydrous ethanol (30.0 ml) and anhydrous acetic acid (3.0 ml).

111  The mixture was sonicated for 30 min to prepare the titanium precursor (labeled as

112  solution A). 6.0 ml anhydrous ethanol and 5.0 ml acetic acid were diluted with 5.0 ml

113  distilled water to get a mixed solution (labeled as solution B). Solution A was stirred

114  vigorously for 30 min at 25□ followed by dropwise addition of solution B to initiate

115  the hydrolysis reaction. The pH value of the mixed solution was controlled by acetic

116    acid. The obtained colloidal solution was stirred for 2 h to form sol, and then aged for

117    12 h to produce the corresponding gelatin. The gelatin was dried at 90□ for 12 h in an

118    oven, then the grayest crystals were obtained. After calcined at 400□ in a flow of

119    nitrogen for 2 h, the obtained powder was magnetic MWCNTs/TiO$_2$ photocatalyst.

120    2.2 Characterization of the catalysts

121        Transmission electron microscope (TEM, JEOL-2010) was used to characterize

122    the morphology of the catalysts and the distribution of γ-Fe$_2$O$_3$ and TiO$_2$ nanoparticles

123    on MWCNTs. The crystalline phase of the synthesized samples was determined by

124    X-ray diffraction (XRD, Phillips PW 1050-3710 Diffractometer) with Cu Kα radiation

125    (λ=1.5406 Å). The magnetization curves of the catalysts were determined by a

126    vibrating sample magnetometer (VSM, Quantum Design MPMS-5S). The surface

127    properties of the catalysts were tested using N$_2$ adsorption-desorption experiments at

128    77 K. The surface area was calculated by the standard Brunauer–Emmett–Teller (BET)

129    equation. All of the calculations were performed using a surface area and porosimeter

130    system (ASAP 2010, Micromeritics). X-ray photo-electron spectroscopy (XPS,

131    Thermo Fisher Scientific) with monochromatic Al Kα X-ray radiation (at 1486.71 eV)

132    was used to identify the oxidation states of the elements in catalysts.

133    2.3 Photocatalytic ozonation experiments
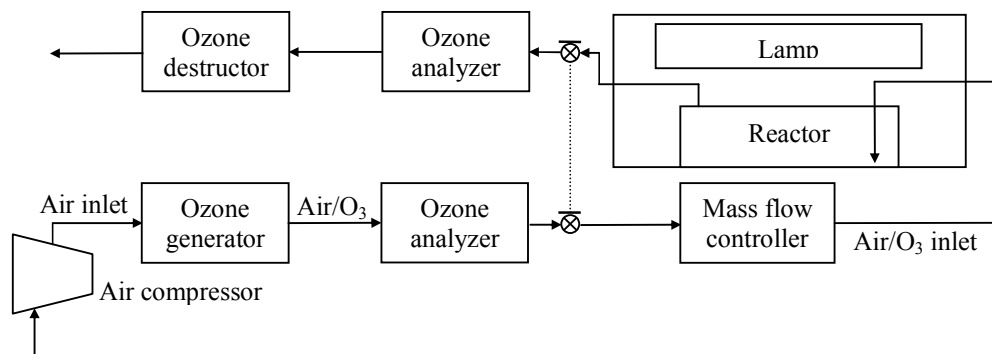
134

135 Fig. 1. Experimental setup for solar photocatalytic ozonation experiments.

136　　　Fig. 1 depicts the schematic of the experimental setup used to carry out

137 ozonation, photocatalytic oxidation and photocatalytic ozonation experiments.

138 Photocatalytic ozonation experiments were conducted in a semi-batch mode, the

139 laboratory-scale system consisted of a 1.0 L glass-made cylindrical reactor, a gas inlet,

140 a gas outlet, and a liquid sampling port. The reactor was placed in a chamber with a

141 commercial solar simulator (Suntest CPS, Atlas), which is a 1500 W air-cooled Xe

142 lamp with emission wavelengths over 300 nm because of the application of quartz and

143 glass cut-off filters. The irradiation intensity was kept at 550 $W/m^2$, and the

144 temperature of the reaction system was maintained between 25 and 40℃ throughout

145 the experiments. If required, an ozone generator (Anseros Ozomat ComAD-02) was

146 used to generate ozone which was supplied to the reactor, the concentration of ozone

147 was recorded with a gas analyzer (Anseros Ozomat GM-6000Pro).

148　　　In a typical photocatalytic ozonation experiment, the reactor was first loaded

149 with 800 ml of aqueous solution containing a certain concentration of the mixture of

150 ATL, HCT, OFX, TMP. Then, 0.2 g of the catalyst was added, and the suspension was

151 stirred in the darkness for 120 min while bubbling air to the system. After this dark

8

152    stage, the Xe lamp was switched on, and simultaneously, a mixture of ozone-oxygen

153    (6.0 mg/L ozone concentration) was fed to the reactor at a flow rate of 20 L/h.

154    Samples were taken from the reactor at specified intervals and filtered through 0.45

155    μm PET membrane to remove the catalyst. Adsorption (i.e. absence of radiation and

156    ozone), single ozonation (i.e. absence of radiation and catalyst), and photolytic

157    oxidation (i.e. absence of radiation, catalyst and ozone) experiments were also carried

158    out for comparative analysis.

159        Concentration of ATL, HCT, OFX and TMP was determined by HPLC with a

160    Waters 2487 UV Detector and Phenomenex Gemini $C_{18}$ column (5 μm, 150 mm×3.0

161    mm). Elution of pharmaceuticals was in gradient form at 0.5 ml/min with two

162    solvents: acidified water (0.1% phosphoric acid) (A) and acetonitrile (B). ATL, TMP,

163    HCT and OFX were detected at 225, 286, 271 and 290 nm with retention times 4.2,

164    9.8, 11.5 and 18.7 min, respectively. The concentration of total phenol was determined

165    by Folin–Ciocalteau method and was expressed as equivalent OFX.[28] TOC was

166    measured by direct injection of filtered samples (Millipore-PVDF 0.45 mm filters)

167    into a TOC analyser (Shimadzu-5050A). Ammonium concentration was determined

168    with a Dionex DX-120 ion chromatograph equipped with a Dionex Ionpac CS12A

169    4×250 mm column. The concentrations of some inorganic anions ($F^-$, $Cl^-$, $NO_3^-$ $NO_2^-$,

170    and $SO_4^{2-}$) and some carboxylates (acetate, oxalate, propionate, formate, maleate and

171    pyruvate) were measured with a Dionex DX-600 ion chromatograph using a Dionex

172    Ionpac AS11-HC 4×250 mm column. The concentration of dissolved ozone was

173    measured by the indigo colorimetric method.[28]

## 3. Results and discussion

3.1. Characterization of the catalysts
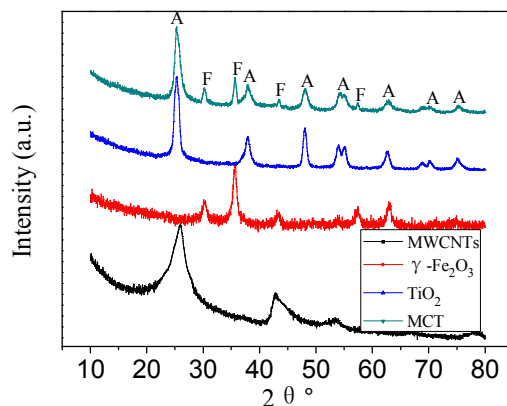


Fig. 2. XRD patterns of MWCNTs, $\gamma$-Fe$_2$O$_3$, TiO$_2$ and magnetic MWCNTs/TiO$_2$ (MCT).

Crystalline phase detected: anatase (A), magnetite/maghemite (F).

Fig. 2 shows the XRD patterns of MWCNTs, $\gamma$-Fe$_2$O$_3$, TiO$_2$ and MCT. The strong graphite peak of plane (002) at $2\theta=25.8°$ can be seen in the XRD patterns of the treated MWCNTs. The other diffraction peaks related to MWCNTs at the angle $2\theta$ of 42.7°, 43.9°, 53.5° and 77.5° can be indexed to the (100), (101), (004) and (110) planes of MWCNTs, suggesting that the structure of MWCNTs was not destroyed after being treated by HNO$_3$. XRD pattern of MCT shows diffraction peaks at 25.4°, 37.9°, 47.9°, 54.4° and 62.8°, which confirms the presence of anatase in the catalyst. $\gamma$-Fe$_2$O$_3$ or Fe$_3$O$_4$ species could also be identified (these two can't be distinguished by XRD) in the XRD patterns of MCT with main diffraction peaks at 30.2°, 35.6°, 43.1° and 57.0°.
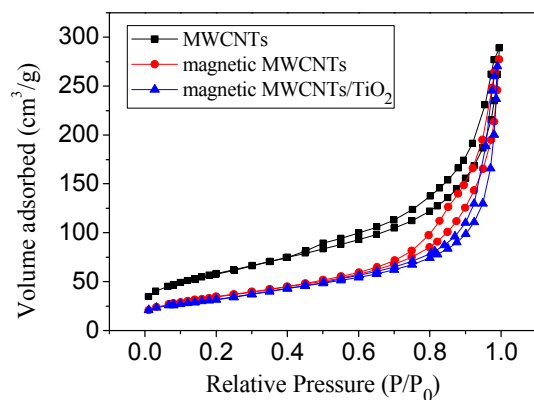
189

190      Fig. 3. Nitrogen adsorption/desorption isotherms of MWCNTs, magnetic MWCNTs and MCT.

191      Fig. 3 shows $N_2$ adsorption/desorption isotherms where it can be noticed that all

192      the three samples displayed type $\square$ isotherms. A wide hysteresis area of the isotherms

193      can be seen in the case of the three samples, suggesting the wide distributions of pore

194      sizes in both cases, this can be due to the agglomeration of MWCNTs, or

195      agglomeration of $\gamma$-$Fe_2O_3$ and $TiO_2$ on the surface of MWCNTs. The pore volume of

196      MCT was lower than that of MWCNTs, which suggests that iron oxides and $TiO_2$

197      nanoparticles might block some pore channels of MWCNTs. The specific surface area

198      of MWCNTs, magnetic MWCNTs and MCT were calculated to be 207.35, 122.27 and

199      $115.81 m^2 g^{-1}$, respectively.



200
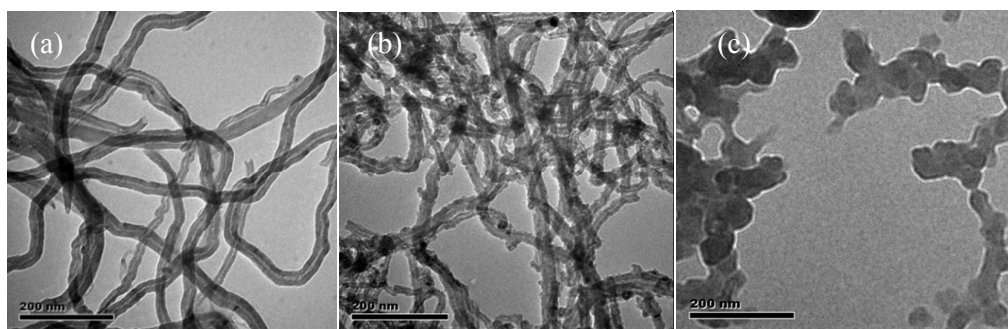
201      Fig. 4. TEM images of the treated MWCNTs (a), $\gamma$-$Fe_2O_3$/MWCNTs (b) and MCT (c).

11

202    Some short MWCNTs can be seen in Fig. 4a, indicating that, in some situations,

203    the damage extended beyond the outermost graphene sheet and into the underlying

204    sidewalls. As can be seen from Fig. 4b, $\gamma$-$Fe_2O_3$ nanoparticles grow around the

205    MWCNTs surface. As shown in Fig. 4c, $TiO_2$ nanoparticles were loaded

206    homogeneously on the surface of magnetic MWCNTs with the diameter of 50-80 nm,

207    most $\gamma$-$Fe_2O_3$ nanoparticles were covered by $TiO_2$ nanoparticles. These results

208    indicated the successful co-incorporation of the two types of nanoparticles on the

209    MWCNTs surface.

210
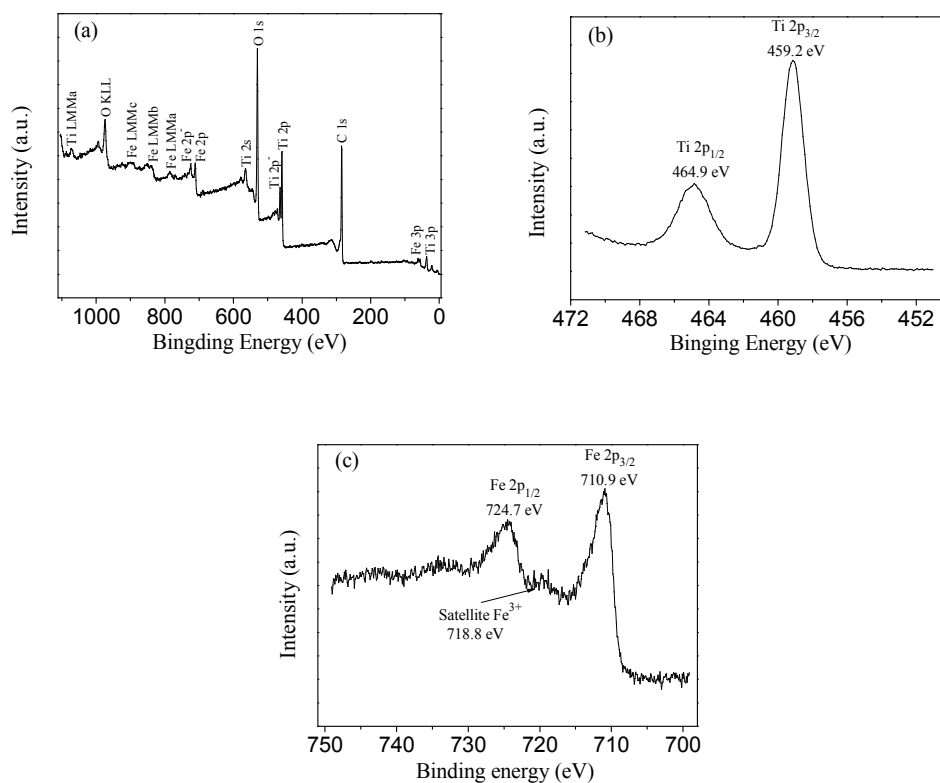
211

212    Fig. 5. XPS full spectrum of magnetic MWCNTs/$TiO_2$ (a), high-resolution XPS spectra of Ti 2p (b)

213                              and Fe 2p (c) spectral regions.

214    Surface chemical composition of the catalyst was analyzed by XPS and the

215    results are presented in Fig. 5. XPS full spectrum of MCT confirmed the presence of

216    C, Ti, O and Fe on the surface of the catalyst (see Fig. 5a). Fig. 5b displays the

217    high-resolution Ti 2p XPS spectrum of the catalyst. The binding energy peaks at 459.2

218    and 464.9 eV can be attributed to the spin-orbit splitting of the Ti 2p components (Ti

219    $2p_{3/2}$ and Ti$2p_{1/2}$), which confirms the presence of Ti as $Ti^{4+}$ ($TiO_2$).[29] Fig. 5c shows

220    the high resolution Fe 2p XPS spectrum of the catalyst. The peaks at 710.9 and 724.7

221    eV can be attributed to Fe $2p_{3/2}$ and Fe $2p_{1/2}$, respectively, indicating the existence of

222    $Fe^{3+}$. In addition, the presence of satellite peak at ca. 718.8 eV further confirmed the

223    existence of $Fe^{3+}$ iron species.[18]
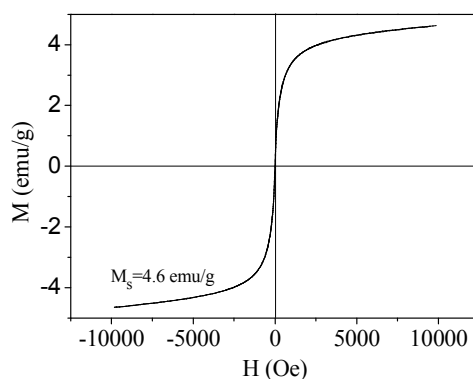


224

225                    Fig. 6. Magnetization vs. applied magnetic field at 25□ of MCT.

226        Fig. 6 illustrates the magnetization hysteresis loop of MCT, the measured

227    saturation magnetization value was 4.63 emu/g, which was weaker than that of

228    $\gamma$-$Fe_2O_3$ (58.83 emu/g). The decrease of the saturation magnetization could be

229    ascribed to the existence of nonmagnetic $TiO_2$ and MWCNTs in MCT. But the

230    saturation magnetization (4.63 emu/g) was still sufficient to achieve fast solid-liquid

231    separation under an external magnetic field. It can also be seen that the catalyst

232    showed zero remanent magnetization and coercitivity, indicating superparamagnetic

233    behavior of the catalyst, so the catalyst could be re-dispersed well in water for reuse

234    after being separated by the external magnetic field.

235    3.2. Ozonation
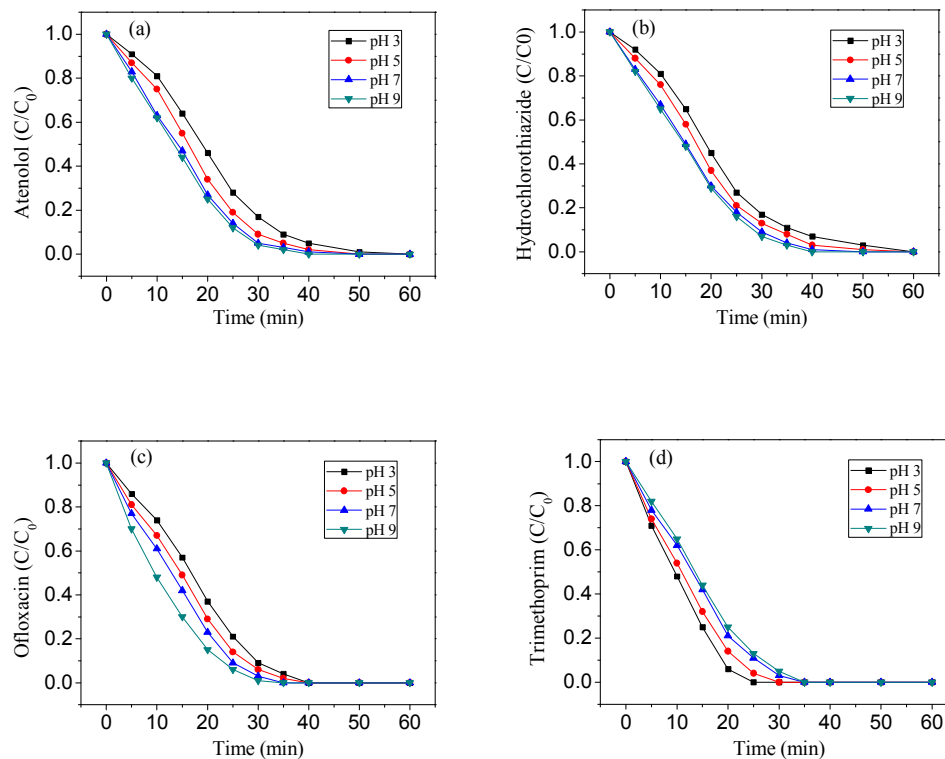


236

237

238    Fig. 7. Degradation of atenolol (a), hydrochlorothiazide (b), ofloxacin (c), trimethoprim (d) by

239    ozonation at pH 3.0-9.0 in aqueous solution. Initial conditions: 800 mL, $[\sum EC]_0$=40 mg/L (10

240    mg/L for each EC), applied ozone mass flow rate, 20.0 L/h, temperature 25±2□.

241    The ozonation experiments were carried out in the pH range of 3.0-9.0. It can be

242    seen from Fig. 7 that pH has an important effect on the ozonation which is due to two

243    contributions: (1) the higher direct ozone reactivity of ionized forms of

244    pharmaceuticals studied (ATL, pKa=9.6; HCT, pKa=7.9; OFX, pKa=6.1, 8.2; TMP,

245 pKa=3.2, 7.1); (2) the possible contribution of hydroxyl radical at elevated pH. In

246 aqueous solution, ATL, HCT, OFX and TMP were completely degraded in 60 min

247 ozonation, as can be observed in Fig. 7 (a-d). ATL, HCT and OFX showed a high

248 degradation rate in alkaline conditions, while TMP showed a high degradation rate in

249 acidic conditions. The difference observed can be explained by the different oxidation

250 mechanisms of ozone. Generally, when the solution pH is below 4.0, the generation

251 of $^{\cdot}$OH is limited and the direct ozonation of organics plays an important role,

252 whereas, both direct ozonation and $^{\cdot}$OH mechanism occur in pH range of 4.0-9.0.

253 When the solution pH is above 9.0, $^{\cdot}$OH generation is predominant.[30,31]

254      Ozone is a selective electrophile and the investigated pharmaceuticals have two

255 reactive sites: aromatic rings and a second amine moiety.[32] As is well known, the

256 reactions between aromatic groups and ozone are independent of the pH.[32] However,

257 the reactions between secondary amine moieties and ozone, or even hydroxyl radicals

258 are pH-dependent (i.e. pKa-dependent), since they are proved to be non-reactive when

259 protonated.[33] The degradation of TMP was unfavorable in alkaline pH. A possible

260 explanation is related to the production of the degradation products, such as organic

261 acids which may compete ozone with TMP, or even the formation of free-radical

262 scavengers which can quench the $^{\cdot}$OH, and these all can reduce the degradation rate of

263 TMP. A similar result was also discovered by Li et al.[34] and Tay et al..[35]

264 3.3. Photocatalytic oxidation

265



266
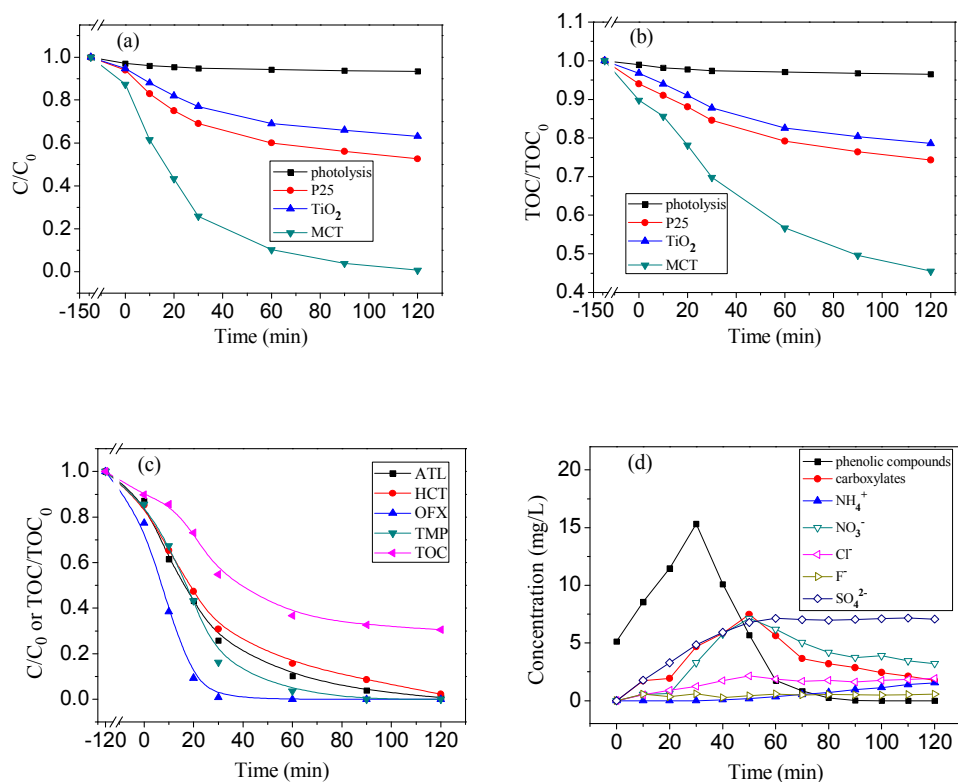
Fig. 8. Time evolution of the concentration of ATL (a) and TOC (b) during photocatalytic

oxidation of a mixture of the four ECs with different catalysts under simulated solar-light radiation

($\lambda$=300-800 nm); Time evolution of the concentration of ATL, HCT, OFX, TMP, TOC (c) and

phenolic compounds ($C_{TP}$), carboxylates ($C_{Carbx}$) and some inorganic ions (d) during

photocatalytic oxidation of a mixture of the ECs in aqueous solution with MCT under simulated

solar-light radiation. Conditions: pH=7.0; $\sum C_{EC0}$=40 mg/L (10 mg/L for each EC); Catalyst

dosage=200 mg/L; average irradiation intensity, 550 W/m$^2$.

As can be seen in Fig. 8a and b, 6.0%, 5.4% and 12.7% of ATL can be removed

by the adsorption of P25, TiO$_2$ and MCT during the darkness stage. It is known that

MWCNTs is a well adsorbent for organic reactants, the higher adsorption capacity of

MCT is due to the MWCNTs in the nanocomposites. The enhanced adsorption

16

278      capacity of the catalysts can lead to an increase in the local concentration of organic

279      matter in the vicinity of their surface,[36] thus promoting surface reactions between

280      adsorbed organic compounds and ·OH. MCT shows higher photocatalytic activity for

281      the removal of ATL and TOC than P25 and $TiO_2$, direct photolysis causes only 6.6%

282      and 3.5% removal efficiencies for ATL and TOC, respectively. ATL was almost

283      completely removed by photocatalytic oxidation with MCT in 120 min, while TOC

284      removal efficiency was just 54.5%, indicating that some intermediates derived from

285      ECs decomposition still remained in solution.

286          As can be seen from Fig. 8c, the photocatalytic oxidation rate followed the order:

287      OFX＞TMP＞ATL＞HCT, and they can be almost completely removed in 120 min

288      by photocatalytic oxidation under simulated solar-light radiation. As can be seen from

289      Fig. 8d, the concentration of phenolic compounds increased up to 15.32 mg/L and

290      then decreased. A similar trend was observed for carboxylates, at the beginning of the

291      process, the concentration of carboxylates increased up to 7.48 mg/L and then

292      decreased. It can be seen that inorganic ions, such as sulphur, chlorine and fluorine

293      can be transformed into sulphate, chloride and fluoride under the experiment

294      conditions.

295      3.4. Photocatalytic ozonation
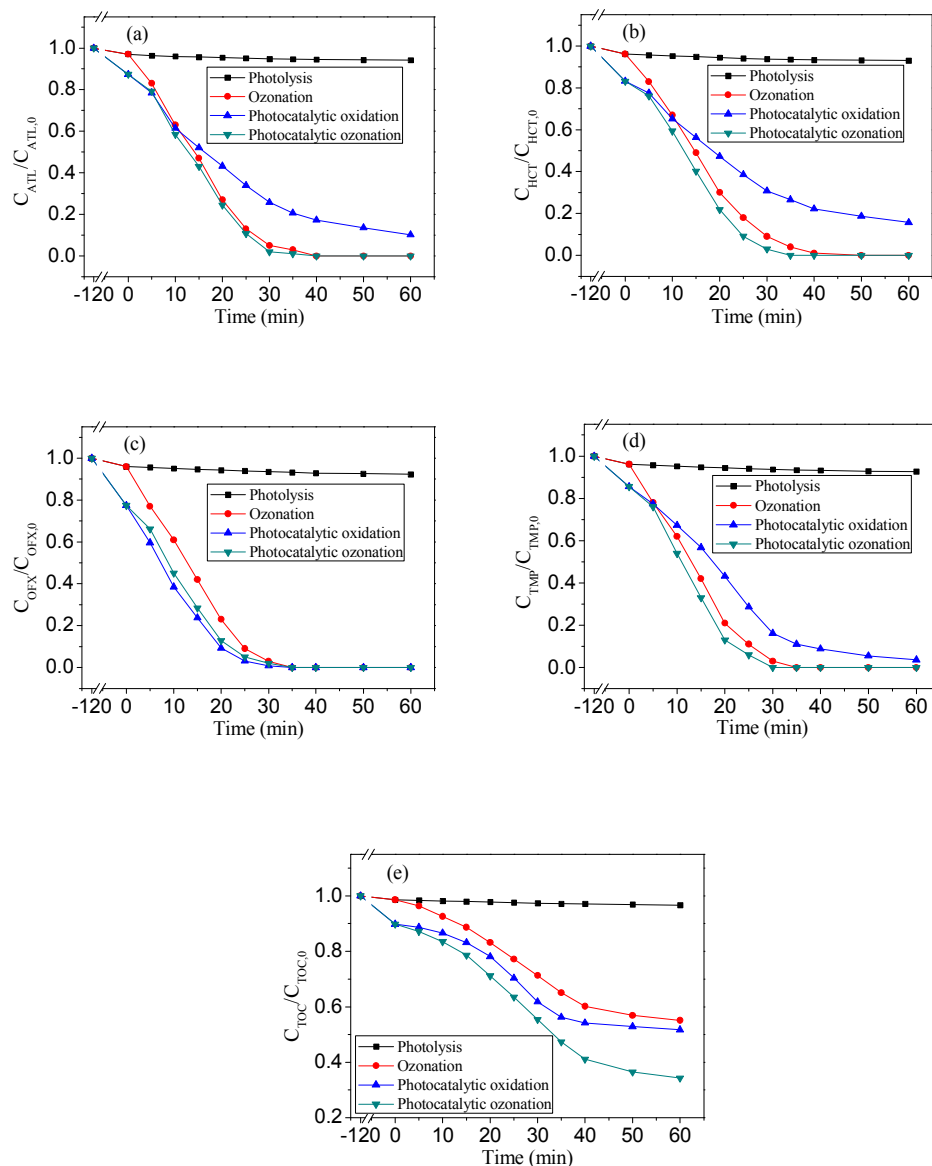
Fig. 9. Time evolution of the concentration of ATL (a), HCT (b), OFX (c), TMP (d) and TOC (e)

during four treatments.

Photocatalytic ozonation experiments were studied and the results were

compared with those obtained from ozonation and photocatalytic oxidation. As can be

seen from Fig. 9, there was not remarkable difference in the removal of all the

pharmaceuticals by ozonation or photocatalytic ozonation, and they led to faster

305    degradation rates of ATL, HCT, TMP than photocatalytic oxidation, which means that

306    direct ozonation was the main reaction pathway in both cases. Similar results have

307    also been observed for ozonation and photocatalytic ozonation of diclofenac and

308    sulfamethoxazole.[19] Although, photocatalytic oxidation was efficient for the removal

309    of OFX, it was not so efficient for the removal of ATL, HCT, TMP and TOC, etc. As

310    can be seen from Fig. 9e, after 60 min of reaction no changes at all was observed in

311    TOC removal in the process of photolysis, while ozonation, photocatalytic oxidation

312    and photocatalytic ozonation allowed 44.9%, 48.3% and 65.7% TOC removal

313    efficiency, respectively (the photocatalytic ozonation data for 120 min can be seen in

314    ESI Fig.2). The photocatalytic ozonation of ECs obeys pseudo-first-order kinetics, the

315    reaction rate constant ($k_{app}$) can be deduced using the following equation[28]:

316    $$-\ln(\frac{C}{C_0}) = k_{app}t \qquad (1)$$

317    where C and $C_0$ are the reactant concentration at time t=t and t=0, respectively.

318    The apparent reaction rate constant for photolysis, ozonation, photocatalytic oxidation

319    and photocatalytic ozonation of TOC are 0.001, 0.011, 0.013 and 0.019 min$^{-1}$,

320    respectively (as can be seen in ESI Fig.1). The highest reaction rate for photocatalytic

321    ozonation can be attributed to the synergism between ozonation and photocatalysis.

322    Ozone, despite being a strong oxidizing agent, reacts selectively with aromatic

323    and unsaturated compounds. As a result of direct ozonation of the pharmaceuticals,

324    non-aromatic and non-unsaturated intermediates compounds are formed (e.g.

325    shortchain carboxylic acids), which react slowly with ozone, they are accumulated in

326    water.[23,24] Photocatalytic ozonation greatly improved the mineralization rate

327     compared to ozonation or photocatalytic oxidation alone, which suggests the

328     existence of some kind of synergism between photocatalytic oxidation and ozonation.

329     First, in the photocatalytic ozonation process, part of ozone can be transformed into

330     hydroxyl radicals (·OH) by the action of MWCNTs,[25,26,29,36] $TiO_2$[36,37] and iron

331     oxides.[36,38] Second, ozone can absorb UV-photons to form excited atomic oxygen

332     species which further generate hydroxyl radicals.[30,31] Third, the photocatalytic effect

333     of anatase (reaction 2) must be considered. This effect can be enhanced by the

334     presence of ozone due to its electrophilic nature, which is prone to trap the electrons

335     generating from the conduction band of $TiO_2$ and then generating ozonide radicals,

336     the generated ozonide radicals can be further transformed into ·OH:[5,6]

337

$$TiO_2 + h\upsilon \rightarrow TiO_2(e^-, h^+) \qquad (2)$$

338

$$O_3 + e^- \rightarrow O_3^{\bullet-} \qquad (3)$$
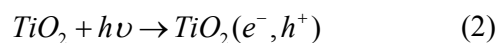
339     The rate constant of reaction (3) is very high[39] and lead to the formation of ·OH

340     through reaction (4):

341

$$O_3^{\bullet-} + H^+ \rightarrow HO_3^{\bullet} \rightarrow {}^{\bullet}OH + O_2 \qquad (4)$$
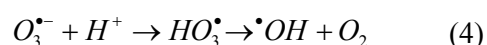
342     **3.5. Catalyst reusability**
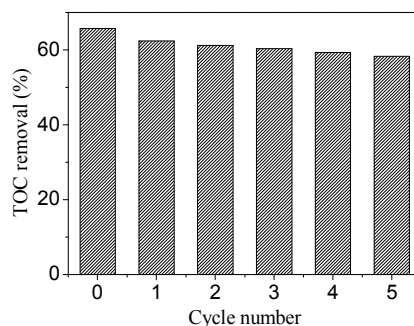


343

344        Fig. 10. TOC conversion for consecutive photocatalytic ozonation runs with MCT.

345    The stability and reusability of MCT were tested by consecutive photocatalytic

346    ozonation experiment. In each run, the catalyst was kept 120 min in the darkness to

347    reach adsorption equilibrium. As can be seen in Fig. 10, there was no evident decrease

348    in catalytic activity for MCT after 5 cycles (65.7%-58.3% TOC removal efficiency),

349    indicating its high durability and stability. After each run, MCT was easily separated

350    from liquid by a magnet.

351    **4. Conclusions**

352    Magnetic MWCNTs/TiO$_2$ synthesized in this work showed well photocatalytic

353    and photocatalytic ozonation activity under simulated solar-light radiation, and the

354    catalyst was successfully applied for the removal of the four ECs existing in urban

355    wastewater through photocatalytic ozonation. The results show that the degradation

356    behaviors of the selected ECs (ATL, HCT, OFX and TMP) when treated with

357    photocatalysis, ozonation and photocatalytic ozonation are very different. Ozone

358    alone is able to almost completely remove the ECs in aqueous solution but the

359    mineralization degree reached is very low (44.7%). As compared to P25 and bare

360    TiO$_2$, MCT showed the best performance in the photocatalytic oxidation process for

361    the removal of ECs. Photocatalytic oxidation led to a TOC removal efficiency of 48.3%

362    in the experimental conditions, but some intermediate products which are difficult to

363    degrade generated during photocatalytic oxidation process. Photocatalytic ozonation

364    was the most efficient for TOC removal (65.7%) and low concentration of

365    intermediates was accumulated during the photocatalytic ozonation process.

366    Synergism between ozonation and photocatalysis was clearly observed in the

367    experiment. From the results of the study, it can be concluded that solar photocatalytic

368    ozonation might be a promising method to remove ECs from water.

369    **Acknowledgements**

374　**References**

375　[1] J. Zhang, B. Sun, X. M. Xiong, N. Y. Gao, W. H. Song, E. Du, X. H. Guan, G. M.

376　　Zhou, Water Res., 2014, 63, 262.

377　[2] A. Bernabeu, R. F. Vercher, L. Santos-Juanes, P. J. Simón, C. Lardín, M. A.

378　　Martínez, J. A. Vicente, R. González, C. Llosá, A. Arques, A. M. Amat, Catal.

379　　Today, 2011, 161, 235.

380　[3] F. Mazille, T. Schoettl, N. Klamerth, S. Malato, C. Pulgarin, Water Res., 2010, 44

381　　3029.

382　[4] D. Fatta-Kassinos, S. Meric, A. Nikolaou, Anal. Bioanal. Chem., 2011, 399, 251.

383　[5] N. Le-Minh, S. J. Khan, J. E. Drewes, R. M. Stuetz, Water Res., 2010, 44, 4295.

384　[6] L. Prieto-Rodriguez, S. Miralles-Cuevas, I. Ollera, P. Fernández-Ibá˜nez, A.

385　　Agüerab, J. Blancoa, S. Malato, Appl. Catal. B: Environ., 2012, 128, 119.

386　[7] M. A. Sousa, C. Gonçalves, J. P. Vilar, A. R. Boaventura, M. F. Alpendurada,

387　　Chem. Eng. J., 2012, 198–199, 301.

388　[8] S. Malato, P. Fernández-Ibanez, M. I. Maldonado, J. Blanco, W. Gernjak, Catal.

389　　Today, 2009, 147, 1.

390　[9] L. Prieto-Rodríguez, I. Oller, N. Klamerth, A. Agüera, E. M. Rodríguez, S. Malato,

391　　Water Res., 2013, 47, 1521.

392　[10] G. Márquez, E. M. Rodríguez, F. J. Beltrán, P. M. Álvarez, Chemosphere, 2014,

393　　113, 71.

394　[11] R. Alimoradzadeh, A. Assadi, S. Nasseri, M. R. Mehrasbi, Iran. J. Environ. Healt.,

395　　2012, 9, 1.

396  [12] T. E. Agustina, H. M. Ang, V. K. Vareek, J. Photochem. Phorobiol., C, 2005, 6,

397      264.

398  [13] E. M. Rodríguez, G. Fernández, P. M. Alvarez, F. J. Beltrán, Water Res., 2012, 46,

399      152.

400  [14] A. Bianco, K. Kostarelos, M. Prato, Chem. Commun., 2011, 47, 10182.

401  [15] J. T. Sun, C. Y. Hong, C. Y. Pan, Polym. Chem., 2011, 2, 998.

402  [16] S. H. Lee, D. H. Lee, W. J. Lee, S. O. Kim, Adv. Funct. Mater., 2011, 21, 1338.

403  [17] X. L. Pan, X. H. Bao, Acc. Chem. Res., 2011, 44, 553.

404  [18] K. Woan, G. Pyrgiotakis, W. Sigmund, Adv. Mater., 2009, 21, 2233.

405  [19] R. Leary, A. Westwood, Carbon, 2011, 49, 741.

406  [20] Y. Yao, G. H. Li, S. Ciston, R. M. Lueptow, K. A. Gray, Environ. Sci. Technol.,

407      2008, 42, 4952.

408  [21] X. Xia, Z. Jia, Y. Yu, Y. Liang, Z. Wang, L. L. Ma, Carbon, 2007, 45, 717.

409  [22] T. J. Bandosz, J. Matos, M. Seredych, M. S. Z. Islam, R. Alfano, Appl Catal A:

410      Gen, 2012, 445, 159.

411  [23] L. F. Velasco, I. M. Fonseca, J. B. Parra, J. C. Lima, C. O. Ania, Carbon, 2012,

412      50, 249.

413  [24] M. A. Andrade, R. J. Carmona, A. S. Mestre, J. Matos, A. P. Carvalho, C. O. Ania,

414      Carbon, 2014, 76, 183.

415  [25] Y. H. Ao, J. J. Xu, D. G. Fu, C. W. Yuan, Carbon, 2008, 46, 596.

416  [26] V. K. Gupta, S. Agarwal, T. A. Saleh, Water Res., 2011, 45, 2207.

417  [27] H. Wang, H. L. Wang, W. F. Jiang, Z. Q. Li, Water Res., 2009, 43, 204.

418 [28] G. Márquez, E. M. Rodríguez, M. I. Maldonado, P. M. Álvarez, Sep. Purif.

419      Technol., 2014, 136, 18.

420 [29] D. H. Quinones, A. Rey, P. M. Álvarez, F. J. Beltrán, P. K. Plucinski, Appl. Catal.

421      B: Environ., 2014, 144, 96.

422 [30] R. Andreozzi, V. Caprio, A. Insola, R. Marotta, Catal. Today, 1999, 53, 51.

423 [31] V. U. Gunten, Water Res., 2003, 37, 1443.

424 [32] J. Benner, E. Salhi, T. A. Ternes, V. U. Gunten, Water Res., 2008, 42, 3003.

425 [33] M. L. Wilde, S. Montipo, A. F. Martins, Water Res., 2014, 48, 280.

426 [34] K. Li, A. Yediler, M. Yang, S. Schulte-Hostede, M. H. Wong, Chemosphere, 2008,

427      72, 473.

428 [35] K. S. Tay, N. A. Rahman, M. R. B. Abas, Chemosphere, 2009, 76: 1296.

429 [36] A. Rey, P. García-Munoz, M. D. Hernández-Alonso, E. Mena, S.

430      García-Rodríguez, F. J. Beltrán, Appl. Catal. B: Environ., 2014, 154–155, 274.

431 [37] H. U. Lee, G. Lee, J. C. Park, Y. C. Lee, S. M. Lee, B. Son, S. Y. Park, C. Kim, S.

432      G. Lee, S. C. Lee, B. Nam, J. W. Lee, D. R. Bae, J. S. Yoon, J. Lee, Chem. Eng.

433      J., 2014, 240, 91.

434 [38] A. Rey, D. H. Quinones, P. M. Álvarez, F. J. Beltrán, P. K. Plucinski, Appl. Catal.

435      B: Environ., 2012, 111–112, 246.

436 [39] E. M. Rodríguez, G. Márquez, E. A. León, P. M. Álvarez, F. J. Beltrán, J.

437      Environ. Manage., 2013, 127, 114.